Antinucleon-nucleon potential

P. H. Timmers, W. A. van der Sanden, and J. J. de Swart
Institute for Theoretical Physics, University of Nijmegen, Nijmegen, The Netherlands
(Received 19 July 1983; revised manuscript received 16 December 1983)

A coupled-channels model for antinucleon-nucleon ($\bar{N}N$) scattering is presented. The $\bar{N}N$ channels are coupled to effective two-particle annihilation channels. The neutron-proton mass difference and the Coulomb interaction are taken exactly into account. This model gives a detailed fit to a set of 977 $\bar{N}N$ scattering data up to $T_{\rm lab}=482$ MeV, with an overall χ^2/data$=1.39$. The potentials are found to be long-ranged. A discussion of several experimental data sets and of the influence of the Coulomb interaction is given.

INTRODUCTION

When the low-energy antiproton ring (LEAR) at CERN comes into operation, the antinucleon-nucleon ($\bar{N}N$) system will be the subject of an extensive experimental investigation.[1] Meanwhile, at the end of this "pre-LEAR" era, one concludes that our knowledge of the $\bar{N}N$ system is very incomplete. On the experimental side, a large set of data points[2–16] is available. However, these are often of limited accuracy and sometimes not consistent with each other. Measurements of observables such as polarizations, spin correlations, etc., are (almost) completely absent. On the theoretical side, several rather phenomenological models exist[17–22] which give a fair description of the available scattering data. Notably lacking here is a coupled-channels model of $\bar{N}N$ scattering. We will present a phenomenological coupled-channels model which gives a rather good description of the currently available low-energy $\bar{N}N$ scattering data up to $T_{\rm lab}=482$ MeV.

In order to get a feeling for the complexity of the $\bar{N}N$ system we compare it for a moment with the rather well-known NN system. In a single-energy proton-proton phase-shift analysis one needs for each total angular momentum J, on the average, 2.5 real parameters (phase shifts δ_J and coupling parameters ϵ_J). In np scattering one needs 5 real parameters for each $J\neq 0$ and 2 for $J=0$. To keep an np phase-shift analysis feasible, one fixes in practice almost all the isospin $I=1$ parameters from the pp scattering data. However, in $\bar{N}N$ scattering (experimentally mainly $\bar{p}p$, i.e., $I=0$ and $I=1$) there is no generalized Pauli principle which excludes in NN for each isospin certain partial waves. Moreover, the phase shifts become complex due to the presence of the strong annihilation. These two features each double the number of required parameters. In $\bar{N}N$ scattering, 20 real parameters are necessary for each $J\neq 0$ and 5 for $J=0$.

Another feature is that the potentials are much stronger in $\bar{N}N$ than in NN. Therefore, more partial waves are contributing significantly to the cross sections at low energies. For example, at $T_{\rm lab}=50$ MeV the percentage of the total cross section due to the s, p, and d waves in np scattering is 87, 7 and 6%, respectively, while in $\bar{p}p$ scattering it is 50, 41, and 9%, respectively. These total cross sections are 164 and 235 mb for np and $\bar{p}p$ scattering, respectively.

The starting point of most theoretical descriptions of $\bar{N}N$ scattering is a certain form of meson-theoretical NN potential, which is G-parity transformed to an $\bar{N}N$ potential. This G-parity transformation reverses the signs of the potential contribution of the odd-G-parity meson exchanges. In the NN potentials large cancellations occur between the contributions of different mesons, e.g., between the repulsive ω-meson contribution and the attractive ϵ-meson contribution. In the $\bar{N}N$ potentials these cancellations no longer occur[23] and these potentials are, in general, very attractive. This has led to speculations about possible $\bar{N}N$ bound states[24–30] and to experiments designed to look for states below the $\bar{p}p$ threshold.[2,3]

The second ingredient in $\bar{N}N$ models is some kind of annihilation mechanism. The annihilation cross section is large ($\sigma_{\rm an}/\sigma_{\rm el}\gtrsim 2$). The $\bar{N}N$ channels are coupled to very many different annihilation channels, most of them multiparticle. The essential characteristic of the $\bar{N}N$ interaction is that it is a many-coupled-channels problem.

Several different approaches for describing the annihilation exist: One may apply a suitable boundary condition,[17,18] use an optical potential,[19–22] or do an actual coupled-channel calculation. A fine example of a boundary-condition model can be found in Ref. 17. This simple model gives, even without including any $\bar{N}N$ potential, a fair description of the total cross section σ_T and of the elastic angular distribution $d\sigma_{\rm el}/d\Omega$ in the forward hemisphere.

If the full coupled-channel problem is understood, one can, in principle, derive an optical potential.[31] However, due to our limited knowledge large simplifications have to be made. In practice, the optical potential is introduced purely "*ad hoc*" or "derived" from some simplified annihilation mechanism like nucleon-exchange.[19,22] A successful optical model was given by Bryan and Phillips.[19] They added to the G-parity-transformed Bryan-Scott NN potential,[32] a very strong imaginary potential. With only two parameters a reasonable description of the scattering data was obtained. The range $R_{\rm eff}$ to which their imaginary potential is effective, is of the order of 1 fm. One

 ©1984 The American Physical Society

of the more recent optical models is that of Côté *et al.*,[22] who use a G-parity-transformed Paris potential, modified in the inner region by a real potential and supplemented by a short-range imaginary potential ($R_{\text{eff}} \lesssim 0.7$ fm). In this model about 20 free parameters are used and a detailed fit to the low-energy data is obtained (χ^2/data$=2.80$). The third way to describe annihilation is to use some kind of coupled-channels model. Because multiparticle annihilation channels may, in principle, be replaced by a weighted set of two-particle channels, we will couple the $\bar{N}N$ channels only to "effective" two-particle annihilation channels. Ultimately one would expect a coupled-channels description of the $\bar{N}N$ system to be closest to reality. From the coupled-channels equations an optical potential can be derived[31] which describes the $\bar{N}N$ sector. This optical potential is generally nonlocal and, in a very specific way, energy- and L-dependent. However, the coupled-channels method provides more information than the optical potential. For example, one can calculate the annihilation cross section for scattering to a specific decay channel. So the inverse process is impossible: one cannot uniquely deduce from an optical potential the coupled-channels equations. Moreover, the required analytic properties and unitarity of the S matrix are automatically guaranteed in a coupled-channels scheme. One has to realize that the problem is far too complicated to take rigorously into account all coupled channels and it remains uncertain whether or not a "truncated" coupled-channels approach is good enough as an approximation. This also applies to the model presented here. However, we show that already two effective decay channels can give a good description of $\bar{N}N$ scattering.

THE MODEL

We will use separate $\bar{p}p$ and $\bar{n}n$ channels. In this way we can take the Coulomb interaction and the *np* mass difference exactly into account.

As diagonal potential in these $\bar{N}N$ channels we use the G-parity-transformed Nijmegen-model-D potential,[33] to which we added a phenomenological shorter-range potential. This Nijmegen-model-D potential is a hard-core baryon-baryon potential, which gives a good fit to the nucleon-nucleon as well as the hyperon-nucleon data. Because of this hard core we must modify the model-D potential in the inner region. We decided to apply a linear cutoff to the model-D $\bar{N}N$ potential, such that

$$V_{\text{nuc}}(r)=\frac{r}{r_c}V_{\text{D}}(r_c) \quad \text{for} \quad 0\le r\le r_c$$
$$=V_{\text{D}}(r) \quad \text{for} \quad r_c\le r \; . \tag{1}$$

Here V_{D} is the G-parity-transformed Nijmegen-model-D potential and r_c is a cutoff radius of the order of the different hard-core radii used in the *BB* potentials. Our choice was $r_c=0.63$ fm. The exchanged mesons with their respective G parity are π $(-)$, η $(+)$, η' $(+)$, ρ $(+)$, ω $(-)$, ϕ $(-)$, ϵ $(+)$.

Next to this model-D potential V_{nuc} we introduce a phenomenological potential of the form

$$V_{\text{ph}}(r)=\left[V_C+V_{\text{SS}}\vec{\sigma}_1\cdot\vec{\sigma}_2+V_T S_{12} m_e r + V_{\text{SO}}\vec{L}\cdot\vec{S}\frac{1}{m_e{}^2 r}\frac{d}{dr}\right]V_{\text{WS}}(r) \tag{2}$$

with

$$V_{\text{WS}}(r)=\frac{1}{1+\exp(m_e r)} \; . \tag{3}$$

As in the case of the linear cutoff applied to V_{D} (1), here too the choice for the tensor potential was motivated by the requirement that the tensor potential should be zero at the origin.

We have introduced in V_{ph} for each isospin four parameters V_C, V_{SS}, V_T, and V_{SO}, which are fitted to the data. The Woods-Saxon form $V_{\text{WS}}(r)$ for the phenomenological potential turned out to be preferred above rapidly falling potentials. The range is determined by the mass m_e, which we choose the same for isospin $I=0$ and $I=1$. The diagonal $\bar{N}N$ potential is thus parametrized by nine real parameters.

The $\bar{N}N$ system is coupled to effective two-particle annihilation channels. The effective particles in the annihilation channel (i,I) are taken to have equal mass M_i and spin zero. The orbital angular momentum l in these effective two-particle channels we take therefore to be $l=J$. For reasons of simplicity we do not assume any interaction between these effective particles in the annihilation channels. For each isospin I only two of these effective annihilation channels are introduced, so $i=1$ and 2. The threshold values of these two channels are not very critical, as long as one is low and the other high, but still below the $\bar{p}p$ threshold. We have chosen these thresholds at $E_T^{(1)}=2M_1=1700$ MeV and $E_T^{(2)}=2M_2=420$ MeV ($\sim 3m_\pi$). It would, physically, not be reasonable if only very specific values of $E_T^{(1)}$ and $E_T^{(2)}$ would allow a fit to the data, since the two annihilation channels have to represent in some average way the very many channels that are actually present. More channels can be included, but while introducing more free parameters, they give no essential improvement of the fit.

The spin-singlet and spin-triplet $\bar{N}N$ channels with $L=J$ are each coupled to four annihilation channels (i,I). For these $L=J$ waves this leads to a 6-coupled-channels problem. These channels are $\bar{p}p$, $\bar{n}n$, and (i,I) with $i=1,2$ and $I=0,1$. The spin-triplet $\bar{N}N$ channels with $L=J\pm 1$ are for each L coupled to four effective annihilation channels. This gives then a 12-coupled-channels system with the channels $\bar{p}p$ $(L=J-1)$, $\bar{p}p$ $(L=J+1)$, $\bar{n}n$ $(L=J-1)$, $\bar{n}n$ $(L=J+1)$, and (i,I,L) with $i=1,2$, $I=0,1$, and $L=J\pm 1$.

The off-diagonal annihilation potential, which couples the $\bar{N}N$ channels with the effective annihilation channels, is parametrized as

$$V_A^{(i,I)}(r)=V(i,I)\frac{1}{1+\exp(m_a r)} \; . \tag{4}$$

In order to minimize the number of parameters we use the same parameters $V(i,I)$ for all $\bar{N}N$ partial waves (L,S,J) and the same range parameter m_a for all annihilation po-

tentials. The total annihilation potential is thus parametrized by only 5 parameters: m_a and $V(i,I)$. The total number of parameters used in the fit is thus 14.

We calculate the scattering parameters by solving the relativistic coupled-channels Schrödinger equation[34–36]

$$(\Delta+p^2-2mV)\psi=0\ . \tag{5}$$

The diagonal matrix p represents the center-of-mass relative momentum and has matrix elements

$$p_{ij}{}^2=\left[\frac{s}{4}-M_i{}^2\right]\delta_{ij}\ , \tag{6}$$

where $\sqrt{s}$ is the total c.m. energy. The diagonal reduced mass matrix m has matrix elements

$$m_{ij}=\tfrac{1}{2}M_i\delta_{ij}\ . \tag{7}$$

The potential matrix V has the form

$$V=\begin{bmatrix} V_{\bar{N}N} & V_A \\ \tilde{V}_A & 0 \end{bmatrix}, \tag{8}$$

where $V_{\bar{N}N}=V_{\rm nuc}+V_{\rm ph}+V_{\rm Coul}$. The Coulomb potential

$$V_{\rm Coul}=-2p\eta'/M_p r$$

has $\eta'=\alpha/v_{\rm lab}$, where $v_{\rm lab}$ is the relative velocity in the laboratory system.[36,37] This accounts for the main part of the relativistic correction to the ordinary Coulomb potential.

RESULTS

The parameters were adjusted to fit the $\bar{p}p$ integrated total and charge-exchange cross sections [$\sigma_T=\sigma(\bar{p}p\to$any) and $\sigma_{\rm CE}=\sigma(\bar{p}p\to\bar{n}n)$] as well as the $\bar{p}p$ differential elastic and charge-exchange cross sections ($d\sigma_{\rm el}/d\Omega$ and $d\sigma_{\rm CE}/d\Omega$). The $\bar{p}p$ integrated elastic cross sections $\sigma_{\rm el}$ were not included in the fit since these are redundant when $d\sigma_{\rm el}/d\Omega$ is given. The values of the 14 parameters are given in Table I.

The bulk of the experimental data included in the fit consist of differential elastic cross sections (846 points), covering the energy range $20\le T_{\rm lab}\le 426$ MeV or momentum range $195\le p_{\rm lab}\le 990$ MeV/c.[4,5,7] This set of data is fitted by our model with χ^2/data=1.31. An example of the quality of this fit is shown in Fig. 1. These measurements of $d\sigma_{\rm el}/d\Omega$, together with some other groups are discussed in more detail in the next section. We would like to mention here explicitly one subset of the elastic cross section. This is the backward elastic cross section $d\sigma_{\rm el}/d\Omega$ measured at $\cos\theta_{\rm c.m.}=-0.994$ by Alston-Garnjost *et al.*[9] They measured at 30 momenta in the range $406\le p_{\rm lab}\le 922$ MeV/c. This set is fitted with χ^2/data=0.98. This fit is shown in Fig. 2.

TABLE I. Potential parameters. The 12 potential strengths are given in MeV and the masses in MeV/c^2. $V(1,I)$ refers to the channels with threshold $E_T^{(1)}=1700$ MeV. $m_e=682.53$, $m_a=425.90$.

	V_C	$V_{\rm SS}$	V_T	$V_{\rm SO}$	$V(1,I)$	$V(2,I)$
$I=0$	−6799	608.9	−992.2	8824	−2021	−5294
$I=1$	−468.5	−433.7	131.1	10468	−1049	−5193

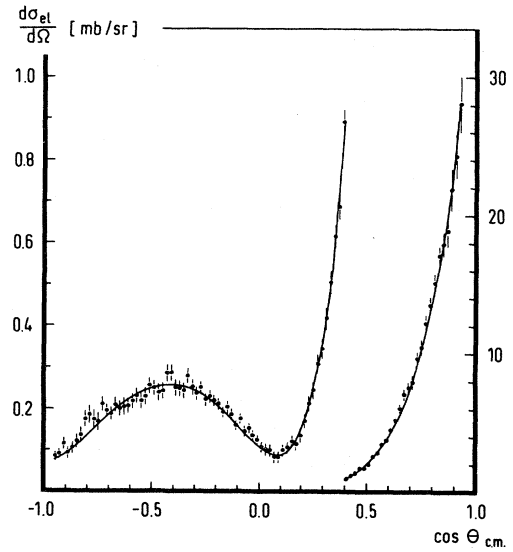

FIG. 1. $\bar{p}p$ elastic differential cross section at $T_{\rm lab}=335$ MeV. Experimental points from Ref. 7 (95 points). Solid curve: model fit (χ^2/data=0.95).

The total cross sections σ_T were taken from Hamilton *et al.*[10] They covered the energy range $65<T_{\rm lab}<482$ MeV or $355<p_{\rm lab}<1066$ MeV/c. In our fit we included only the data up to 426 MeV. These cross sections are corrected for the pure Coulomb and the Coulomb-nuclear interference contributions. The whole set (including the data with $T_{\rm lab}>426$ MeV) has, with respect to our model, χ^2/data=1.21. However, some care should be taken with this χ^2. We could not take the systematic errors (which are larger than the statistical errors) exactly into account, since their origin and momentum dependence were not

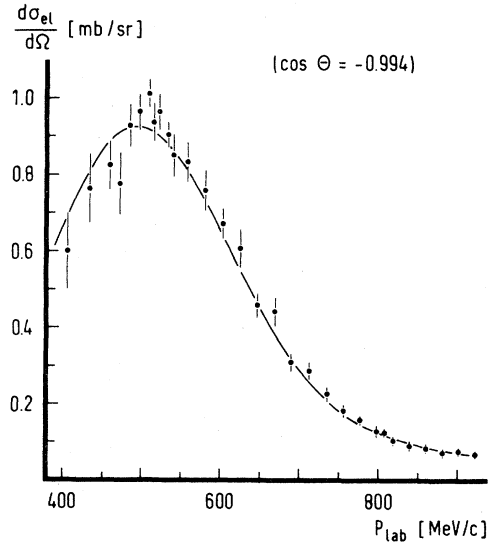

FIG. 2. $\bar{p}p$ backward elastic cross section vs $p_{\rm lab}$. Experimental points from Ref. 9. Solid curve: model fit.

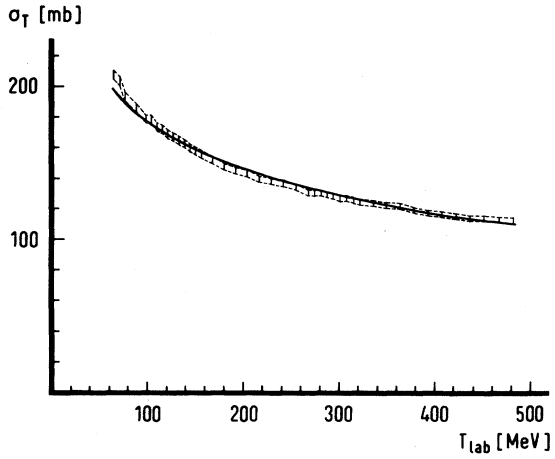

FIG. 3. $\bar{p}p$ total cross section vs T_{lab}. Band: representation of the experimental data from Ref. 10 (see text). Solid curve: model fit.

known. For this reason we present in Fig. 3 the experimental data by a band, covering the range of the systematic errors. The total cross section as calculated by us (solid curve) lies almost everywhere inside this band.

The same way of presenting the data was chosen for the charge-exchange cross sections σ_{CE}, shown in Fig. 4 together with our fit. These 52 data points in the range $23 \leq T_{lab} \leq 467$ MeV or $208 \leq p_{lab} \leq 1046$ MeV/c (Ref. 13) are fitted with a χ^2/data$=2.85$. In general, the shape of our curve is different from what is suggested by the experimental data. At low energies the threshold effect is much stronger in our model than in the currently available data.

A few measurements exist of $d\sigma_{CE}/d\Omega$ at 93 and 149 MeV (Ref. 14), and at 230 MeV.[6] They are fitted with χ^2/data$=1.28$. An example of this fit is shown in Fig. 5. The bump-dip observed here in the forward direction can be simulated with the one-pion-exchange amplitude (in first Born approximation) and a constant background amplitude.[38,39]

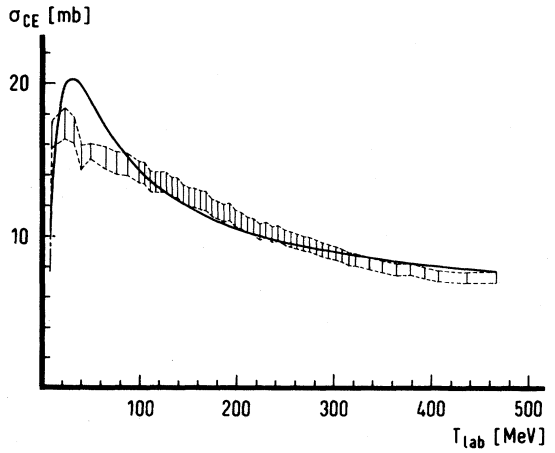

FIG. 4. $\bar{p}p$ charge-exchange cross section vs T_{lab}. Band: representation of the experimental data from Ref. 12 (see text). Solid curve: model fit.

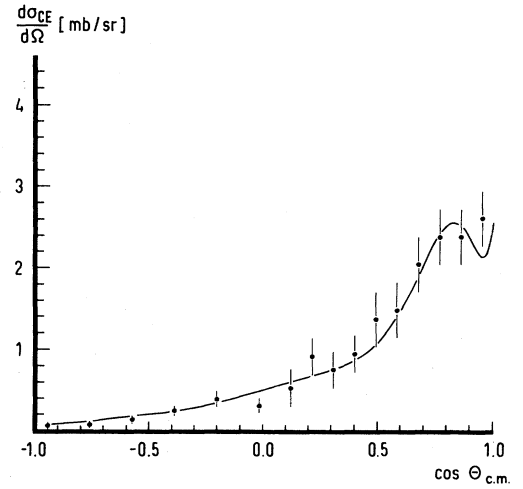

FIG. 5. $\bar{p}p$ charge-exchange differential cross section at $T_{lab}=230$ MeV. Experimental points from Ref. 6. Solid curve: model fit.

Very little is known about polarizations in $\bar{p}p$ elastic scattering. The few measurements at $T_{lab}=230$ MeV (Refs. 15 and 16) were not included in the fit, but our prediction has χ^2/data$=0.46$. The polarization at this energy is shown in Fig. 6, together with the experimental data.

The total number of data included in the fit is 977. For this whole set of data our fit has χ^2/data$=1.39$. Since the differential elastic cross sections constitute the majority of them, the total χ^2 is mainly determined by the χ^2 for these data.

EXPERIMENTS

First we discuss here five groups of measurements of $d\sigma_{el}/d\Omega$. The characteristics of these groups are given in Table II. The groups 1, 2, and 4 were included in the fitting procedure, the results of which are given in the previous section.

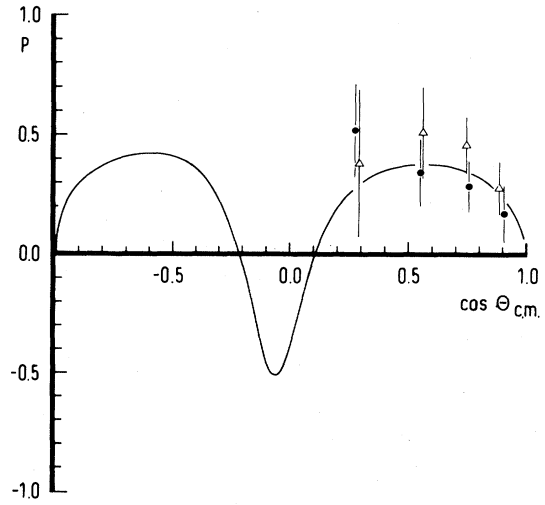

FIG. 6. $\bar{p}p$ polarization at $T_{lab}=230$ MeV. Triangles: Ohsugi *et al.* (Ref. 15). Circles: Kimura *et al.* (Ref. 16). Solid curve: prediction of the model.

TABLE II. Experiments on $d\sigma_{el}/d\Omega$.

Group	Ref.	Range T_{lab} (MeV)	Points	χ^2/data
1	4	20–70	118	2.48
2	5	63–175	329	1.05
3	6	230	21	0.89
4	7	226–426	374	1.20
5	8	369	19	5.60

Group 1 is made up of 118 data points measured by Spencer and Edwards at six energies (20, 30, 40, 50, 60, and 70 MeV). For this group we used a 4% normalization error. This set of data was fitted with χ^2/data=2.48. In general, our fit to this group tends to be somewhat flat compared to experiment. This effect is strongest at the lowest energy. The points at 20 MeV have χ^2/data=4.93. Inspection of the S-matrix elements seems to indicate that the waves with $L>0$ are too weak at these energies. Also, at 60 MeV, a comparably high χ^2 is found: χ^2/data=2.74. Here the backward points contribute most. However, these data are quite far ($\sim 3\sigma$) off from those of the second group.

Group 2 consists of 329 data points measured by Conforto *et al.* in the energy range $62.7 \leq T_{lab} \leq 175$ MeV. A normalization error of 4% was assumed for these data too. A problem with these data is that for small values of the cross section the authors quote as the error on $d\sigma_{el}/d\Omega$ the value of this cross section. This even leads to the extreme case $d\sigma_{el}/d\Omega = 0.0 \pm 0.0$. The simplest way to deal with these points would be to leave them out altogether. However, we did take them into account after replacing the errors of these points by the more reasonable errors quoted for neighboring points. In this way 50 out of 329 data points are corrected. Another difficulty, in the cases where only a small number of events is counted, is that the use of a Gaussian probability distribution is not quite appropriate. However, for the sake of simplicity we stick to it in the determination of χ^2. We obtain for this set χ^2/data=1.05. In determining this χ^2, two points at 99.8 MeV were removed (at $\cos\theta = -0.075$ and $\cos\theta = 0.175$). These two isolated points have a high χ^2, while their surrounding points have typically $\chi^2 \lesssim 1.0$. We only rejected points if the total set of points where they stem from is fitted with $\chi^2/d \approx 1$ if the points are isolated, and if their individual χ^2 contribution is at least 12. The latter criterion is modeled after Chauvenet's criterion, that the total probability of occurrence of all deviations equally large or larger does not exceed $1/2n$, where $n=977$ is the total number of points included in the fit.[40]

Group 3 consists of 21 data points measured by Kohno *et al.* at $T_{lab}=230$ MeV. This set has χ^2/data=0.89. In our fitting procedure we did not include this group, because the better quality data from group 4 were available at this energy.

Group 4 consists of accurate data by Eisenhandler *et al.* In our fit we included the data at $T_{lab}=226$, 288, 335, and 426 MeV. In this set, too, a few points are found which were rejected on the critera stated above (one point at 226 MeV, $\cos\theta=0.37$ and two points at 426 MeV with $\cos\theta = -0.69$ and 0.25, respectively). Our fit to the remaining 371 data points yields χ^2/data=1.20.

Well within the extremes of energy of group 4 is an older set of $d\sigma_{el}/d\Omega$ data at $T_{lab}=369$ MeV (group 5). This older group gives a high χ^2/data=5.60. We conclude that this group is in conflict with group 4 and we therefore omitted this group from our data set.

Data on $d\sigma_{CE}/d\Omega$ are scarce. The experiment by Bizarri *et al.*[14] at $T_{lab}=93$ and 149 MeV is fitted with χ^2/data=1.75. The experiment from Kohno *et al.*[15] at $T_{lab}=230$ MeV has somewhat better statistics. Our fit here has χ^2/data=0.70.

Our model gives on the 43 data points of Hamilton *et al.*[10] on σ_T a χ^2/data=1.21. A measurement of σ_T was also done by Chaloupka *et al.*[11] This set of 18 data points with energies between 49 and 150 MeV has, with respect to our model, χ^2/data=8.23. This group, however, shows a resonant structure around 125 MeV which is clearly not present in our model. Besides, at the low-energy side these data also deviate about 2σ from those of Hamilton *et al.*

DISCUSSION

A characteristic of this coupled-channel model for $\bar{N}N$ scattering is that the potentials have a long "range." We determined this range by making the annihilation potential V_A zero outside a certain radius. For example, when we set $V_A(r)=0$ for $r \geq 1.0$, 1.5, and 2.0 fm we find at $p_{lab}=600$ MeV/c a total cross section of $\sigma_T=142.9$, 146.3, and 159.3 mb, respectively, whereas the complete potential gives $\sigma_T=152.7$ mb. The "effective range" R_{eff}, i.e., the value of the radius r outside which the potential V_A will change the cross sections by about 5–10%, is in the order of 1.5 fm for the annihilation potential. The same range is found for V_{ph}. This potential seems to represent more than only the inner part of the nuclear potential V_{nuc}. This long range is contrary to the findings of Ref. 22. We feel that the data also indicate a long range of the interaction. This can be seen, e.g., in the forward peak of the differential cross sections (which are fitted very well in our model). The peak can be parametrized with a one-pole term: $d\sigma/dt \propto (t+\mu^2)^{-2}$. The higher the mass μ, the broader the peak will be. Typically, one estimates $\mu \approx 270$ MeV/c^2. From the low-t behavior of the annihilation potential in our model one obtains

$$\mu_A = (426/\sqrt{2})\ \text{MeV/c}^2 = 301\ \text{MeV/c}^2 .$$

One would then expect that models which have a larger mass determining the annihilation will show a forward differential cross section which is too flat. Accurate measurements of these forward cross sections might then give a tool to discriminate between various models.

The contributions of the partial waves to σ_T, σ_{el}, and σ_{CE} at five momenta are given in Table III. Note the dominant contribution to σ_T and σ_{el} of the $N\bar{N}$ triplet-coupled waves. We define here σ_{el} as the elastic cross section for $\bar{p}p$ scattering, without the pure Coulomb contribution and with the Coulomb-nuclear interference term integrated up to $\cos\theta=0.975$. The total cross section σ_T is taken to be the "nuclear" contribution to σ_T, i.e., no

TABLE III. Partial-wave cross sections. $\sigma_A^{(1)}$ is the annihilation cross section to the channels with threshold $E_T^{(1)}=1700$ MeV.

p_{lab} (MeV/c)	200	400	600	800	1000
$^1S_0$	7.33	5.60	3.60	2.28	1.54
$^3S_1+^3D_1$	91.31	43.13	19.79	9.72	5.77
$^3P_0$	0.79	0.63	1.45	1.68	1.56
$^1P_1$	0.09	1.65	3.52	3.96	3.51
$^3P_1$	1.85	4.76	5.10	4.40	3.44
$^3P_2+^3F_2$	6.44	17.84	16.81	12.15	8.35
$^1D_2$	0.04	0.35	1.02	1.57	1.72
$^3D_2$	0.10	0.40	1.26	1.85	1.89
$^3D_3+^3G_3$	0.02	1.61	6.20	8.01	7.23
$^1F_3$	0.01	0.06	0.19	0.45	0.71
$^3F_3$	0.00	0.05	0.07	0.31	0.69
$^3F_4+^3H_4$	0.00	0.06	0.51	1.65	3.17
$^1G_4$	0.00	0.01	0.04	0.09	0.18
$^3G_4$	0.00	0.02	0.03	0.02	0.07
$^3G_5+^3I_5$	0.00	0.01	0.05	0.20	0.82
rest	0.00	0.00	0.04	0.10	0.23
σ_{el} (mb)	107.97	76.18	59.70	48.45	40.88
$^1S_0$	4.99	1.27	0.59	0.43	0.38
$^3S_1+^3D_1$	4.18	2.84	1.72	1.38	1.31
$^3P_0$	4.19	2.59	1.41	0.95	0.68
$^1P_1$	0.82	0.19	0.12	0.24	0.33
$^3P_1$	4.38	3.57	1.58	0.83	0.49
$^3P_2+^3F_2$	0.84	1.57	0.99	0.67	0.58
$^1D_2$	0.11	0.41	0.37	0.31	0.23
$^3D_2$	0.30	1.60	1.39	0.87	0.50
$^3D_3+^3G_3$	0.03	0.69	1.14	1.21	1.22
$^1F_3$	0.01	0.13	0.27	0.37	0.38
$^3F_3$	0.02	0.36	0.55	0.41	0.31
$^3F_4+^3H_4$	0.00	0.12	0.33	0.34	0.13
$^1G_4$	0.00	0.03	0.08	0.13	0.19
$^3G_4$	0.00	0.08	0.23	0.26	0.19
$^3G_5+^3I_5$	0.00	0.02	0.12	0.21	0.39
rest	0.00	0.04	0.20	0.39	0.51
σ_{CE} (mb)	19.86	15.51	11.10	9.00	7.82
$^1S_0$	23.31	10.41	6.13	3.94	2.76
$^3S_1+^3D_1$	146.46	63.87	30.92	16.86	10.90
$^3P_0$	5.53	3.76	3.46	3.27	2.80
$^1P_1$	5.76	6.98	7.98	7.82	6.88
$^3P_1$	16.04	17.13	13.11	10.03	7.65
$^3P_2+^3F_2$	59.38	51.25	35.53	24.07	16.77
$^1D_2$	1.84	7.09	8.57	7.93	6.84
$^3D_2$	1.50	6.82	9.47	8.96	7.48
$^3D_3+^3G_3$	2.67	15.70	24.83	22.55	17.99
$^1F_3$	0.05	0.90	2.94	4.76	5.38
$^3F_3$	0.04	0.93	2.59	4.29	5.24
$^3F_4+^3H_4$	0.05	1.16	5.24	9.65	11.66
$^1G_4$	0.00	0.08	0.44	1.15	1.99
$^3G_4$	0.00	0.13	0.52	1.07	1.73
$^3G_5+^3I_5$	0.00	0.11	0.56	1.87	5.13
rest	0.00	0.04	0.39	1.14	2.44
σ_T (mb)	262.64	186.40	152.68	129.34	113.63
$\sigma_A^{(1)}$ (mb)	108.46	73.10	60.79	50.73	43.78

pure Coulomb or Coulomb-nuclear interference terms are included in σ_T. However, the nuclear amplitude is determined by taking the Coulomb interaction exactly into account. This means that the (relativistic) Coulomb potential was included and that the wave functions were adjusted to Coulomb wave functions in the asymptotic region.

In optical models, sometimes another procedure is followed (see, e.g., Ref. 19). One then calculates the nuclear amplitude as if no Coulomb interaction at all was present. The total cross section is determined from this amplitude by means of the optical theorem. In Table IV we compare at three energies the two methods for determining σ_T. One sees that large differences can occur, increasing when the energy T_{lab} is lowered. In those optical models the differential cross sections are determined by attaching Coulomb phases to the above mentioned nuclear amplitude and adding the Coulomb amplitude to it. A comparison of this method with the exact method, used by us, can be seen in Fig. 7 for $T_{\text{lab}}=62.7$ MeV. Displayed here is the differential elastic cross-section in which the pure Coulomb contribution has been subtracted. This corrected cross section can become negative due to the large negative Coulomb-nuclear interference term.

When we compare our results with those of Côté *et al.*,[22] taking about the same set of data, we have on this set $\chi^2/\text{data}=1.49$, whereas their optical model yielded $\chi^2/\text{data}=2.80$. In our fit we included more points, at high energies, and excluded one set of data on $d\sigma_{\text{el}}/d\Omega$ at 369 MeV,[8] which gave our final $\chi^2/\text{data}=1.39$.

ACKNOWLEDGMENTS

We wish to thank Dr. T. A. Rijken for stimulating discussions and Dr. R. D. Tripp for sending us numerical values of his results. Part of this work was included in the research program of the Stichting voor Fundamenteel Onderzoek der Materie (FOM) with financial support from the Nederlandse Organisatie voor Zuiver-Wetenschappelijk Onderzoek (ZWO).

APPENDIX

The relativistic Schrödinger equation for total angular momentum J is

$$\left[\frac{d^2}{dr^2}+p^2-\frac{L^2}{r^2}-2mV^J\right]\chi^J(r)=0\ ,$$

where p^2, L^2, m, V^J, and χ^J are matrices in channel space. On the particle basis we label the channels by $(LSM\alpha)$, where α indicates the type of particles ($\bar{p}p$, $\bar{n}n$, ...). For example, the matrix elements of L^2 are

TABLE IV. Total cross section in millibarns, exact and without Coulomb distortion (see text).

T_{lab} (MeV)	Exact	No distortion
20	269.35	251.96
50	212.01	205.33
100	177.17	174.00

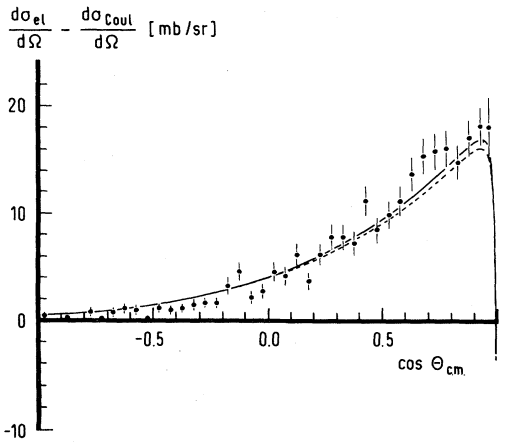

FIG. 7. $(d\sigma_{\text{el}}/d\Omega)-(d\sigma_{\text{Coul}}/d\Omega)$ at $T_{\text{lab}}=62.7$ MeV in $\bar{p}p$ scattering. Experimental data from Ref. 5. Solid curve: with Coulomb distortion. Dashed curve: without Coulomb distortion.

$$(L^2)_{L'S'M'\alpha',LSM\alpha}=L(L+1)\delta_{L'L}\delta_{S'S}\delta_{M'M}\delta_{\alpha'\alpha}\ .$$

The above given particle channels are not the isospin eigenstates for the $\bar{N}N$ sector. The transformation matrix between particle basis and isospin basis is in this sector:

$$U_{\bar{N}N}=U_{\bar{N}N}^{-1}=\frac{1}{\sqrt{2}}\begin{bmatrix}1 & 1\\ 1 & -1\end{bmatrix}.$$

On the isospin basis V^J looks like

$$V^J=\begin{bmatrix}V^J_{\bar{N}N} & V^J_A\\ \tilde{V}^J_A & \sigma\end{bmatrix}$$

with

$$V^J_A=\begin{bmatrix}V_A^{(1,0)} & 0 & V_A^{(2,0)} & 0\\ 0 & V_A^{(1,1)} & 0 & V_A^{(2,1)}\end{bmatrix}$$

with $V_A^{(i,I)}$ given in Eq. (4), and $V^J_{\bar{N}N}=V^J_{\text{nuc}}+V^J_{\text{ph}}+V_{\text{Coul}}$, where (in the $\bar{N}N$ sector)

$$V^J_{\text{nuc}}=\begin{bmatrix}V^J_{0,\text{nuc}} & 0\\ 0 & V^J_{1,\text{nuc}}\end{bmatrix}$$

and likewise V^J_{ph}. $V^J_{I,\text{nuc}}$ is the isospin$=I$, total angular momentum$=J$ part of the V_{nuc} from Eq. (1).

On the particle basis, in the $\bar{N}N$ sector $(\bar{p}p,\bar{n}n)$ the Coulomb potential is

$$V_C(r)=\begin{bmatrix}\dfrac{-2p\eta'}{M_p r} & 0\\ 0 & 0\end{bmatrix}.$$

Also on the particle basis in the $\bar{N}N$ sector the reduced mass matrix

$$m=\begin{bmatrix}m_{\bar{p}p} & 0\\ 0 & m_{\bar{n}n}\end{bmatrix}=\tfrac{1}{2}\begin{bmatrix}M_p & 0\\ 0 & M_n\end{bmatrix}$$

and the center-of-mass relative momentum

$$p^2=\begin{bmatrix} p_{\bar{p}p}{}^2 & 0 \\ 0 & p_{\bar{n}n}{}^2 \end{bmatrix}=\begin{bmatrix} \frac{S}{4}-M_p{}^2 & 0 \\ 0 & \frac{S}{4}-M_n{}^2 \end{bmatrix}.$$

The asymptotic form of the regular wave function χ^J is

$$\chi^J(r) \underset{r\to\infty}{\sim} \left[\frac{m}{p}\right]^{1/2}(F+GK^J)A^J .$$

Here F and G are diagonal matrices on the particle basis:

$$(F)_{LSM\alpha,LSM\alpha}=F_L(\eta'_\alpha,p_\alpha r) ,$$

$$(G)_{LSM\alpha,LSM\alpha}=G_L(\eta'_\alpha,p_\alpha r) ,$$

where F_L and G_L are, respectively, the standard regular and irregular Coulomb wave functions.

The partial-wave S matrix S^J is

$$S^J=(1+iK^J)(1-iK^J)^{-1} .$$

The matrix A^J is dependent upon the boundary conditions chosen for $\chi^J(r)$.

The scattering amplitude $M=M^N+M^C$, where the nuclear amplitude is

$$M^N(S'm'\alpha'\leftarrow Sm\alpha;\hat{p}_{\alpha'})=\sum_{JLL'}[4\pi(2L+1)]^{1/2}C^{L\ S\ J}_{0\ m\ m}C^{L'\ S'\ J}_{m-m'\ m'\ m}Y^{L'}_{m-m'}(\hat{p}_{\alpha'})e^{i\sigma^{\alpha'}_{L'}}\left[\frac{S^J-1}{2ip_\alpha}\right]_{L'S'm'\alpha',LSm\alpha}e^{i\sigma^{\alpha}_{L}}$$

with $\vec{p}_\alpha=p_\alpha\hat{z}$ and $\hat{p}_{\alpha'}$ is a unit vector in the direction of $\vec{p}_{\alpha'}$.

The Coulomb amplitude is

$$M^C(S'm'\alpha'\leftarrow Sm\alpha;\hat{p}_{\alpha'})=\frac{\eta'_\alpha}{2p_\alpha\sin^2\frac{\theta}{2}}\exp\left[i\eta'_\alpha\ln\left[\sin^2\frac{\theta}{2}\right]+2i\sigma^\alpha_0\right]\delta_{S'S}\delta_{m'm}\delta_{\alpha'\alpha}$$

$(\hat{p}_{\alpha'}\cdot\hat{p}_\alpha=\cos\theta)$.

Observables are calculated from the amplitude M, e.g.,

$$\frac{d\sigma_{CE}}{d\Omega}=\frac{d\sigma}{d\Omega}(\bar{n}n\leftarrow\bar{p}p)=\tfrac{1}{4}\sum_{\substack{sm\\ s'm'}}|M(S'm',\bar{n}n\leftarrow Sm,\bar{p}p)|^2 \quad \text{(for unpolarized } \bar{p}p) .$$

[1]See, e.g., K. Killian, in *Proceedings of the Fifth European Symposium on Nucleon-Antinucleon Interactions, Bressanone, Italy, 1980* (Instituto Nazionale Fisica Nucleare, Padua, 1980), p. 681.

[2]T. E. Kalogeropoulos and G. S. Tzanakos, Phys. Rev. Lett. 34, 1047 (1975).

[3]P. Pavlopoulos *et al.*, Phys. Lett. 72B, 415 (1978); Report No. CERN-EP/82-177 (unpublished).

[4]D. Spencer and D. N. Edwards, Nucl. Phys. B19, 501 (1970).

[5]B. Conforto *et al.*, Nuovo Cimento 54A, 441 (1968).

[6]H. Kohno *et al.*, Nucl. Phys. B41, 485 (1972).

[7]E. Eisenhandler *et al.*, Nucl. Phys. B113, 1 (1976).

[8]M. G. Albrow *et al.*, Nucl. Phys. B37, 349 (1972).

[9]M. Alston-Garnjost *et al.*, Phys. Rev. Lett. 43, 1901 (1979).

[10]R. P. Hamilton *et al.*, Phys. Rev. Lett. 44, 1182 (1980).

[11]V. Chaloupka *et al.*, Phys. Lett. 61B, 487 (1976).

[12]R. J. Abrams *et al.*, Phys. Rev. D 1, 1917 (1970).

[13]R. P. Hamilton *et al.*, Phys. Rev. Lett. 44, 1179 (1980).

[14]R. Bizarri *et al.*, Nuovo Cimento 54A, 456 (1968).

[15]T. Ohsugi *et al.*, Nuovo Cimento 17A, 456 (1973).

[16]M. Kimura *et al.*, in *Proceedings of the Fourth European Symposium $\bar{N}N$ Interactions, Strasbourg, France, 1978,* edited by A. Fridman (Editions du Centre National de la Recherche Scientifique, Paris, 1979), p. 539.

[17]A. Delville, P. Jasselette, and J. Vandermeulen, Am. J. Phys. 46, 907 (1978).

[18]O. D. Dalkarov and F. Myhrer, Nuovo Cimento 40A, 152 (1977).

[19]R. A. Bryan and R. J. N. Phillips, Nucl. Phys. B5, 201 (1968).

[20]C. B. Dover and J. M. Richard, Phys. Rev. C 21, 1466 (1980).

[21]T. Ueda, Prog. Theor. Phys. 62, 1670 (1979).

[22]J. Côté *et al.*, Phys. Rev. Lett. 48, 1319 (1982).

[23]W. W. Buck, C. B. Dover, and J. M. Richard, Ann. Phys. (N.Y.) 121, 47 (1979); C. B. Dover and J. M. Richard, *ibid.* (N.Y.) 121, 70 (1979).

[24]I. S. Shapiro, Phys. Rep 35C, 129 (1978).

[25]A. M. Badalyan, M. I. Polykarpov, and Yu. A. Simonov, Phys. Lett. 76B, 277 (1978).

[26]M. van der Velde, Ph.D. thesis, Vrije Universiteit Amsterdam, 1980.

[27]F. Myhrer and A. Gersten, Nuovo Cimento 37A, 21 (1977).

[28]J. A. Tjon, Phys. Rev. D 18, 2565 (1978).

[29]F. Myhrer and A. W. Thomas, Phys. Lett. 64B, 59 (1976).

[30]C. B. Dover and M. Goldhaber, Phys. Rev. D 15, 1997 (1977).

[31]H. Feshbach, Ann. Phys. (N.Y.) 5, 357 (1958); 19, 287 (1962).

[32]R. A. Bryan and B. L. Scott, Phys. Rev. 135, B434 (1964).

[33]M. M. Nagels, T. A. Rijken, and J. J. de Swart, Phys. Rev. D 12, 744 (1975).

[34]Erkelenz, Phys. Rep. C13, 191 (1974).

[35]J. J. de Swart and M. M. Nagels, Fortschr. Phys. 28, 215 (1978).

[36]G. J. M. Austen and J. J. de Swart, Phys. Rev. Lett. 50, 2039 (1983).

[37]G. Breit, Phys. Rev. 99, 1581 (1955).

[38]E. Leader, Phys. Lett. 60B, 290 (1976).

[39]H. Bogdanski *et al.*, Phys. Lett. 62B, 117 (1976).

[40]L. G. Parrat, *Probability and Experimental Errors in Science* (Wiley, New York, 1961).